

Modulation instability in the nonlinear Schrödinger equation with a synthetic magnetic field: Gauge matters

Lelas, Karlo; Čelan, Ozana; Prelogović, David; Buljan, Hrvoje; Jukić, Dario

Source / Izvornik: **Physical Review A, 2021, 103**

Journal article, Published version

Rad u časopisu, Objavljena verzija rada (izdavačev PDF)

<https://doi.org/10.1103/PhysRevA.103.013309>

Permanent link / Trajna poveznica: <https://um.nsk.hr/um:nbn:hr:217:005512>

Rights / Prava: [In copyright](#) / [Zaštićeno autorskim pravom.](#)

Download date / Datum preuzimanja: **2024-10-14**



Repository / Repozitorij:

[Repository of the Faculty of Science - University of Zagreb](#)



Modulation instability in the nonlinear Schrödinger equation with a synthetic magnetic field: Gauge matters

Karlo Lelas,^{1,*} Ozana Čelan², David Prelogović³, Hrvoje Buljan,² and Dario Jukić^{4,†}

¹*Faculty of Textile Technology, University of Zagreb, Prilaz baruna Filipovića 28a, 10000 Zagreb, Croatia*

²*Department of Physics, Faculty of Science, University of Zagreb, Bijenička c. 32, 10000 Zagreb, Croatia*

³*Scuola Normale Superiore, Piazza dei Cavalieri 7, I-56126 Pisa, Italy*

⁴*Faculty of Civil Engineering, University of Zagreb, A. Kačića Miošića 26, 10000 Zagreb, Croatia*



(Received 27 March 2020; accepted 15 December 2020; published 12 January 2021)

We theoretically investigate the phenomenon of modulation instability for systems obeying the nonlinear Schrödinger equation, which are under the influence of an external homogeneous synthetic magnetic field. For an initial condition, the instability is detected numerically by comparing dynamics with and without a small initial perturbation; the perturbations are characterized in a standard fashion by wave vectors in momentum space. We demonstrate that the region of (in)stability in momentum space, as well as time evolution in real space, for identical initial conditions, depend on the choice of the gauge (i.e., vector potential) used to describe the homogeneous synthetic magnetic field. This superficially appears as if the gauge invariance is broken, but this is not true. When the system is evolved from an identical initial condition in two different gauges, it is equivalent to suddenly turning on the synthetic magnetic field at $t = 0$. This gives rise, via Faraday's law, to an initial instantaneous kick of a synthetic electric field to the wave packet, which can differ for gauges yielding an identical uniform magnetic field for $t > 0$.

DOI: [10.1103/PhysRevA.103.013309](https://doi.org/10.1103/PhysRevA.103.013309)

I. INTRODUCTION

Modulation instability (MI) is a nonlinear phenomenon which has been long studied in various physical systems including fluid dynamics, nonlinear optics, and plasma physics [1–10] (for historical overview of early work, see Ref. [11]). Following major experimental developments with ultracold atomic gases, MI has been investigated for Bose-Einstein condensates (BECs) [12–15]. MI occurs when small perturbations on the uniform background intensity become exponentially amplified. In this way instability, which develops from the interplay of nonlinearity and dispersion [10], breaks the symmetry of the uniform state. As a recent example, experiments with ultracold atoms have investigated the role of MI in the formation of matter-wave solitons [16,17], in analogy with extensive studies of solitons in optics [18]. In this paper we explore MI in a nonlinear system with a synthetic magnetic field.

The implementation of synthetic gauge fields is of great interest in atomic systems [19,20], because it can enable exploring topological phases of matter [21]. Analogous ideas on photonic platforms have led to the emergence of topological photonics [22,23]. There is extensive literature on synthetic gauge fields and topological phases in these systems, as some of the ideas arose a quarter of a century ago [24]; a number of comprehensive reviews on these topics [19–23], some of which are very recent [21,23], have been published.

Let us mention a few of the schemes used for the creation of synthetic gauge fields for atoms [25–32] and photons [33–36]. The first scheme for ultracold atoms was implemented in rapidly rotating BECs by employing the analogy between the Coriolis and the Lorentz force [25,26]. The first implementation using light-atom interaction employed the analogy between the Aharonov-Bohm phase for charged particles, and the Berry phase for ultracold atoms with spatially dependent Raman coupling between internal hyperfine states [27]. Very successful schemes were implemented in optical lattices [28–32], where the tunneling matrix element between neighboring sites is engineered to acquire a synthetic Peierls phase.

An equivalent strategy to engineer coupling between optical cavities, or photonic lattice sites, has been proposed in photonic systems (e.g., see Refs. [37–41]). It was successfully implemented by using link resonators of different length [35], to image topological edge states [35]. A scheme mimicking strained graphene was used in photonic lattices to obtain artificial magnetic fields [33]. Interestingly, photonic Floquet topological insulators were implemented using helical waveguides which yield synthetic electric fields [34]. A non-Abelian gauge field has been synthesized recently in an optical setup [36].

A majority of work on synthetic gauge fields and topological phases are in noninteracting systems (single-particle phenomena) for ultracold atoms [19–21], and in linear photonic systems [22,23]. However, when interactions or nonlinearity are turned on, intriguing phenomena such as the fractional quantum Hall effect can emerge [42,43]. The nonlinear photonic phenomena addressed in the topological

*klelas@tff.unizg.hr

†djukic@grad.unizg.hr

context include an analysis of the Hofstadter butterfly in a nonlinear Harper lattice [44], solitons [45–49], nonlinear harmonic generation [50,51], topological lasers [52–54], topological transitions [55,56], nonlinear control [57], and nonlinear pumping [58] of topological edge states.

In this paper, we theoretically explore how the implementation of the homogeneous synthetic magnetic field in systems modeled by the two-dimensional (2D) nonlinear Schrödinger equation (NLSE) affects the MI phenomenon. Dynamics of weakly interacting BECs (in the mean-field approximation) and propagation of light through nonlinear media are both described by the NLSE [10,59]; for BECs it is usually referred to as the Gross-Pitaevskii equation (GPE) [59]. Therefore, our study is applicable to both ultracold atomic and photonic systems. In two dimensions, the addition of an external uniform magnetic field into a Hamiltonian leads to harmonic terms (among others) in the NLSE, resembling the scalar harmonic trap potential. For this reason, in Sec. II we first outline the study of MI in one-dimensional (1D) harmonic traps, following the work in Ref. [15]. The NLSE in 2D with a magnetic field is introduced in Sec. III for different gauges of the vector potential. In Sec. IV we numerically explore MI in 2D NLSE with the synthetic magnetic field. More specifically, we explore the time evolution of an initial Thomas-Fermi profile wave packet (with and without perturbations), and compare its dynamics for symmetrical and Landau gauges. Perturbations are characterized in momentum space. We demonstrate that the dynamics of wave packets with identical initial conditions, and regions of (in)stability in momentum space, are dependent on the choice of the gauge. This may seem as if gauge invariance is broken; however, this is not true. When the system is evolved from an identical initial condition in two different gauges yielding the same uniform synthetic magnetic field, it is equivalent to suddenly turning on the field at $t = 0$ (or $z = 0$ in spatial photonics). At this instance, fields arising from gauges differ and our results can be explained with Faraday's law: as the homogeneous synthetic magnetic field is turned on, an instantaneous kick of a synthetic electric field, which differs in the two gauges, occurs and affects subsequent dynamics. This *gauge matters* effect has already been noted in Ref. [60] in a different context. Finally, in Sec. V we conclude and summarize our results.

II. MODULATION INSTABILITY IN 1D NLSE WITH HARMONIC POTENTIAL

We start by studying a 1D system in a harmonic potential which satisfies the dimensionless NLSE,

$$i \frac{\partial \psi}{\partial t} = \left(-\frac{\partial^2}{\partial x^2} + ax^2 + \eta |\psi|^2 \right) \psi. \quad (1)$$

Here, a is the harmonic oscillator constant, and $\eta < 0$ characterizes the strength of the nonlinearity. Due to the harmonic potential, this equation does not have a homogeneous ground state for which a standard MI analysis could be performed. This problem has been thoroughly studied in Ref. [15] numerically.

For clarity, we will briefly review a demonstration of MI in this system. We assume that the initial state is the ground state of the stationary NLSE in the Thomas-Fermi (TF)

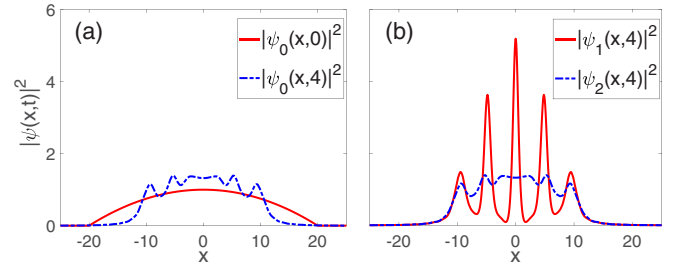


FIG. 1. Modulation instability in 1D NLSE with a harmonic potential. (a) Density of the initial state $\psi_0(x, 0) = \psi_{\text{TF}}$ (solid red line) and density of the time-evolved state $\psi_0(x, 4)$ (dashed blue line). (b) Densities of the time-evolved states $\psi_1(x, 4)$ (solid red line) and $\psi_2(x, 4)$ (dashed blue line), obtained with time evolution of the perturbed initial states $\psi_1(x, 0) = \mathcal{N}_1 \psi_{\text{TF}}(1 + 0.01 \cos x)$ and $\psi_2(x, 0) = \mathcal{N}_2 \psi_{\text{TF}}(1 + 0.01 \cos 2x)$, respectively. See text for details. (Here and throughout the paper all plotted quantities are dimensionless.)

approximation. The stationary equation reads

$$\mu \psi = \left(-\frac{\partial^2}{\partial x^2} + ax^2 + \eta' |\psi|^2 \right) \psi, \quad (2)$$

where μ is the chemical potential, and the nonlinearity is positive, $\eta' > 0$. In the TF approximation the kinetic energy term is neglected, and the resulting wave function is $\psi_{\text{TF}} = \sqrt{\frac{\mu - ax^2}{\eta'}}$ for $|x| < \sqrt{\mu/a}$, and $\psi_{\text{TF}} = 0$ elsewhere. We choose the chemical potential $\mu = 1$, harmonic oscillator constant $a = 0.0025$, and strength of the nonlinearity $\eta' = 1$ [15]. Since MI is expected to occur at negative values of nonlinearity, we quench the system so that the sign of nonlinearity is switched from positive η' to negative $\eta = -\eta'$ at $t = 0$, and investigate the time evolution of Eq. (1) with the TF initial condition. In the context of ultracold atomic gases, this quench in the nonlinearity can be achieved experimentally by using Feshbach resonances [61].

The time dynamics of the initial state $\psi_0(x, 0) = \psi_{\text{TF}}$, which we observe after the quench, results in density modulations, shown in Fig. 1(a) at $t = 4$, but they are here present only due to the fact the TF state is not an eigenstate of the system. On the other hand, MI is demonstrated by studying the time evolution of a slightly perturbed initial TF state. In our calculations, the perturbed initial states are of the form $\psi_k(x, 0) = \mathcal{N}_k \psi_{\text{TF}}(1 + \cos kx)$, where $k = \{1, 2\}$, and the constant \mathcal{N}_k ensures that both perturbed initial states have the same normalization as the unperturbed initial TF state. As visible in Fig. 1(b), adding an appropriate noise term with $k = 1$ leads to density modulations which develop quickly in time, indicating that the initial state is unstable with respect to the perturbation with $k = 1$. In contrast, the perturbation with $k = 2$ does not destabilize the trajectory from the initial TF state, as visible in Fig. 1(b). At this point, it is worth noting that at long times the TF state (which is not equal to the ground state of the case with $\eta = -1$) will eventually be destroyed, i.e., large amplitude localized excitations will be developed independently of the initial value of k , due to the excitation of unstable momenta [15].

III. TWO-DIMENSIONAL NLSE WITH A SYNTHETIC MAGNETIC FIELD: WHICH GAUGE TO USE?

Imagine the following experiment. We have a 2D photonic system with an implemented synthetic magnetic field and the Kerr type nonlinearity. We launch a beam with some initial profile into this system and ask whether the trajectory from this initial condition is stable or not. For a definition of stability of trajectories which are not periodic please see Ref. [62], the section on Lyapunov exponents. In the paraxial approximation this system is modeled with the NLSE. An equivalent experiment in BECs would be to prepare the weakly interacting BEC in some initial state, in a potential confining the dynamics to two dimensions; then, we suddenly turn on the synthetic magnetic field, and wonder whether subsequent dynamics is sensitive to small perturbations on the initial state.

This is modeled with the NLSE in 2D with an additional vector potential \mathbf{A} ,

$$i\frac{\partial\psi}{\partial t} = [(-i\nabla - \mathbf{A})^2 + \eta|\psi|^2]\psi, \quad (3)$$

where $\nabla = \hat{x}\frac{\partial}{\partial x} + \hat{y}\frac{\partial}{\partial y}$ and $\psi \equiv \psi(x, y, t)$. In photonics, the ‘‘time variable’’ is the propagation axis coordinate z instead of t [23]. The vector potential \mathbf{A} corresponds to a homogeneous synthetic magnetic field perpendicular to the 2D plane, $\mathbf{B} = B\hat{z} = \nabla \times \mathbf{A}$. We should have the freedom to choose a gauge for the vector potential \mathbf{A} and focus on two most common choices, the symmetric and the Landau gauge.

In the symmetric gauge $\mathbf{A}_S = \frac{1}{2}B(-y\hat{x} + x\hat{y})$, which leads to the following time-dependent NLSE in 2D:

$$i\frac{\partial\psi}{\partial t} = \left[-\frac{\partial^2}{\partial x^2} - \frac{\partial^2}{\partial y^2} - iBy\frac{\partial}{\partial x} + iBx\frac{\partial}{\partial y} + \frac{1}{4}B^2(x^2 + y^2) + \eta|\psi|^2 \right] \psi. \quad (4)$$

We can write the Landau gauge either as $\mathbf{A}_{Lx} = -By\hat{x}$ or $\mathbf{A}_{Ly} = Bx\hat{y}$. With the choice \mathbf{A}_{Lx} , the time-dependent NLSE reads

$$i\frac{\partial\psi}{\partial t} = \left(-\frac{\partial^2}{\partial x^2} - \frac{\partial^2}{\partial y^2} - 2iBy\frac{\partial}{\partial x} + B^2y^2 + \eta|\psi|^2 \right) \psi, \quad (5)$$

and with \mathbf{A}_{Ly} we have

$$i\frac{\partial\psi}{\partial t} = \left(-\frac{\partial^2}{\partial x^2} - \frac{\partial^2}{\partial y^2} + 2iBx\frac{\partial}{\partial y} + B^2x^2 + \eta|\psi|^2 \right) \psi. \quad (6)$$

It is obvious that dynamics from an identical initial condition $\psi(x, y, t = 0)$ will differ if we evolve it in a different gauge, i.e., evolution with Eqs. (4), (5), or (6) will differ. However, this does not mean that the gauge invariance principle is violated. Equations (4), (5), and (6) are related through gauge transformations of the vector potential. However, in order for all three of them to yield the same dynamics, the initial condition for one of them should be $\psi(x, y, 0)$, and the initial conditions for the other two should be appropriately gauge transformed. Because the system is experimentally prepared in the state $\psi(x, y, 0)$ at $t = 0$, it is not immediately clear which equation, that is, which gauge to use for this initial condition.

To understand what happened, note that in the gedanken experiments described above, in the photonic and BEC context, the system is prepared in some state, and then at $t = 0$ the synthetic magnetic field is suddenly turned on (in photonics this is the moment the optical beam enters the 2D medium). Thus, $B(t) = B\theta(t)$, and the vector potential $\mathbf{A}(x, y, t) = \mathbf{A}(x, y)\theta(t)$, where $\theta(t)$ is the Heaviside step function. By Faraday’s law, the synthetic magnetic field at the instant $t = 0$ creates a spatially dependent synthetic electric field kick, which differs for the gauges mentioned above. We obtain the following electric fields in different gauges: $\mathbf{E}_S = -\frac{\partial\mathbf{A}_S}{\partial t} = -B\delta(t)(-\frac{y}{2}\hat{x} + \frac{x}{2}\hat{y})$, $\mathbf{E}_{Lx} = -\frac{\partial\mathbf{A}_{Lx}}{\partial t} = B\delta(t)y\hat{x}$, and $\mathbf{E}_{Ly} = -\frac{\partial\mathbf{A}_{Ly}}{\partial t} = -B\delta(t)x\hat{y}$. Thus, even though at times $t > 0$ the fields generated by the vector potential are identical, this kick affects dynamics for times $t > 0$.

One can ask next, which gauge should we use for a given experiment? This depends on the experiment and the way synthetic magnetic field is implemented at $t = 0$. A given implementation of the uniform synthetic magnetic field will have a particular and unique synthetic electric field kick at $t = 0$. The gauge used for the dynamics should yield exactly the same synthetic electric field kick in order to describe the experimental situation. In the next section we will discuss the MI phenomenon in the aforementioned different gauges, which as we have just explained correspond to different experimental implementations of the field. Before that let us elaborate how we choose the initial condition and explore MI.

When we introduce the vector potential into NLSE, new terms on the right-hand side of Eqs. (4)–(6) appear: first-order spatial partial derivatives and harmonic confinement terms. Due to the harmonic terms, we do not proceed with the standard MI analysis by using plane wave as an initial state, because plane waves are not eigenstates of any of Eqs. (4)–(6). However, following the discussion from the previous section, for the initial state we choose the ground state of the 2D NLSE with isotropic harmonic confinement $\frac{1}{4}B^2(x^2 + y^2)$

$$\mu\psi = \left[-\frac{\partial^2}{\partial x^2} - \frac{\partial^2}{\partial y^2} + \frac{1}{4}B^2(x^2 + y^2) + \eta'|\psi|^2 \right] \psi, \quad (7)$$

in the TF approximation. We choose $\mu = 1$ for the chemical potential, the field is set to $B = 0.1$, and the strength of the nonlinearity is positive, $\eta' = 1$. In the TF approximation we neglect the kinetic energy terms, which leads to the ground state wave function

$$\psi_{\text{TF}}(x, y) = \sqrt{\frac{\mu - \frac{1}{4}B^2(x^2 + y^2)}{\eta'}} \quad (8)$$

for $0 < \sqrt{x^2 + y^2} < 2\frac{\sqrt{\mu}}{B}$, and $\psi_{\text{TF}} = 0$ elsewhere. We observe the time evolution of the system from this initial state; we propagate it with Eq. (3) with nonlinearity $\eta = -\eta'$, because the MI is expected in the regime of negative nonlinearities (attractive BECs or self-focusing nonlinear media).

IV. MODULATION INSTABILITY IN 2D NLSE WITH A SYNTHETIC MAGNETIC FIELD

In this section, we present numerical results which demonstrate MI in our system. For this, we have implemented a 2D split-step method for the time evolution with the NLSE

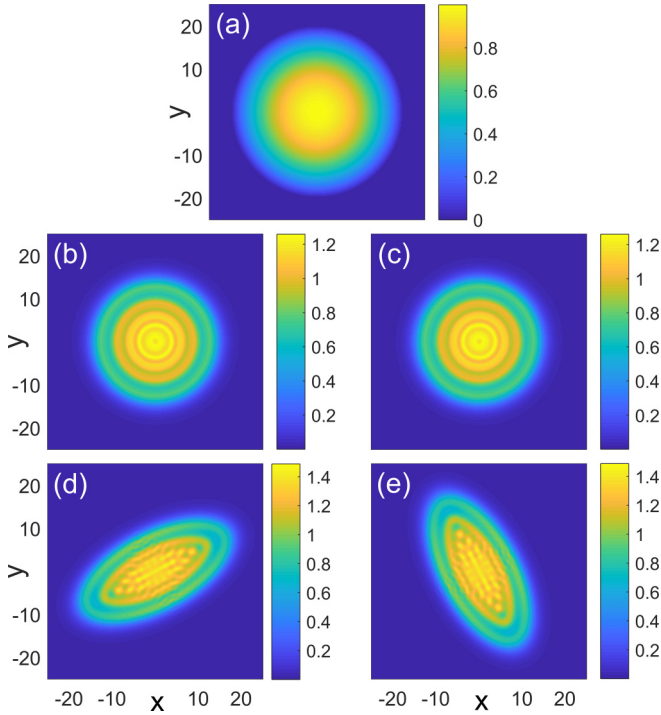


FIG. 2. (a) Density $|\psi_{00}(x, y, 0)|^2 = |\psi_{\text{TF}}|^2$ of the initial Thomas-Fermi state (8). Density $|\psi_{00}(x, y, t = 3)|^2$ evolved with (b) the harmonic potential only [Eq. (9)], (c) the symmetric gauge \mathbf{A}_S [Eq. (4)], (d) the Landau gauge \mathbf{A}_{Lx} [Eq. (5)], and (e) the Landau gauge \mathbf{A}_{Ly} [Eq. (6)].

(3) in the symmetric and the Landau gauge, which include the first-order spatial partial derivatives and harmonic terms arising from the vector potential. For comparison, we will also show results for the time evolution of the NLSE with only the harmonic terms present, that is, for 2D generalization of Eq. (1),

$$i \frac{\partial \psi}{\partial t} = \left[-\frac{\partial^2}{\partial x^2} - \frac{\partial^2}{\partial y^2} + \frac{1}{4} B^2 (x^2 + y^2) + \eta |\psi|^2 \right] \psi. \quad (9)$$

The initial state $\psi_{00}(x, y, 0) = \psi_{\text{TF}}$ given in (8) is illustrated in Fig. 2(a). The time evolution of this state propagated in different gauges [Eq. (9) and Eqs. (4)–(6)] is presented in Figs. 2(b)–2(e). We observe that small density modulations develop in time because the initial TF state is not an eigenstate of the system in any gauge. The time evolution with only the harmonic term present (9), and with the magnetic field in the symmetric gauge (4) are hardly distinguishable for the chosen set of parameters [compare Figs. 2(b) and 2(c)]. In the Landau gauge(s) the density cloud becomes elongated and rotated in time [Figs. 2(d) and 2(e)]. The two density clouds in Figs. 2(d) and 2(e) are oriented at $\pi/2$ angle relative to each other, which reflects the geometric relationship between Landau gauges \mathbf{A}_{Lx} and \mathbf{A}_{Ly} .

We now add perturbations to the initial state,

$$\psi_{k_x k_y}(x, y, 0) = \mathcal{N}_{k_x k_y} \psi_{\text{TF}} [1 + 0.01 \cos(k_x x + k_y y)]. \quad (10)$$

Here, $\mathbf{k} = (k_x, k_y)$ is a 2D momentum of the perturbation, and $\mathcal{N}_{k_x k_y}$ is the normalization constant such that perturbed TF states have the same normalization as the unperturbed TF state

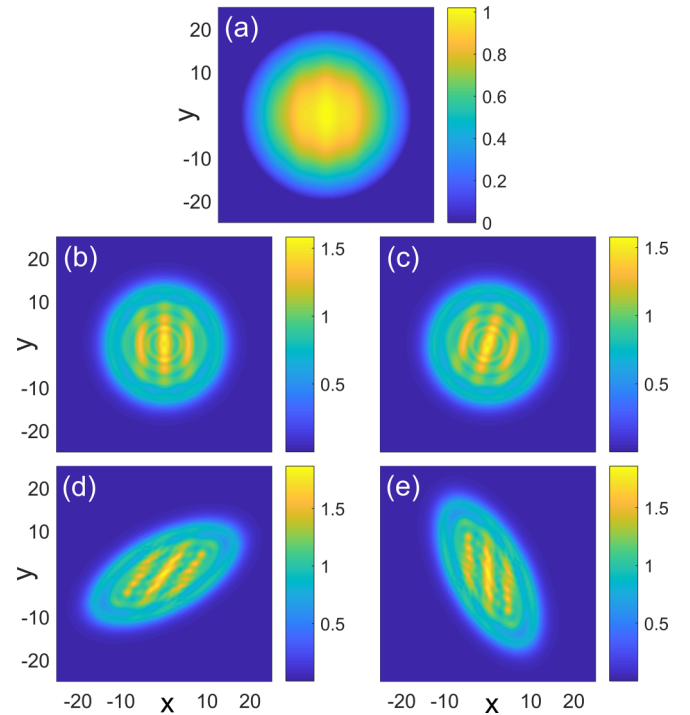


FIG. 3. (a) Density $|\psi_{10}(x, y, 0)|^2$ of initial state (10) with perturbation momentum ($k_x = 1, k_y = 0$). (b)–(e) Density $|\psi_{10}(x, y, t = 3)|^2$ evolved with the same equations as in Figs. 2(b)–2(e).

(8). In order to consistently compare the time evolution of the perturbed (10) and unperturbed initial state (8) we show time-evolved density profiles at $t = 3$. We emphasize that, similarly as in the 1D example, the dynamics for longer times will eventually lead to the destruction of the TF cloud in all cases, i.e., generation of very strongly localized patterns due to the presence of unstable momenta in the initial TF state. For the set of parameters chosen in our calculations, the subsequent collapse of the wave function will also be observed. However, here we study instability that occurs at short timescales, rather than the long-term behavior of the wave packet. Therefore we can exploit the separation of timescales, i.e., the time for which the MI phenomenon can be established occurs prior to the destruction and collapse of the TF state.

First, we consider $\psi_{10}(x, y, 0)$ with perturbation momentum $(k_x, k_y) = (1, 0)$. The density profile of this initial state is shown in Fig. 3(a), and its time evolution in different gauges in Figs. 3(b)–3(e); the outlines of Figs. 2 and 3 are identical for easier comparison. We see that in all gauges the MI is present, as can be seen from the strong modulations in the densities. Time evolution with the harmonic confinement only [Eq. (9)], and with the symmetric gauge [Eq. (4)] show MI with the same intensity modulations [Figs. 3(b) and 3(c)]; however, in the symmetric gauge we observe rotation of modulation patterns. In the Landau gauge \mathbf{A}_{Lx} [Eq. (5)], both the density cloud and its modulation patterns are elongated and rotated in time [Fig. 3(d)]. In contrast, in the Landau gauge \mathbf{A}_{Ly} [Eq. (6)], the cloud is also elongated and rotated, but modulation patterns do not rotate during the time evolution [Fig. 3(e)]. This difference in the modulation patterns in Landau gauges reflects the differences between synthetic electric

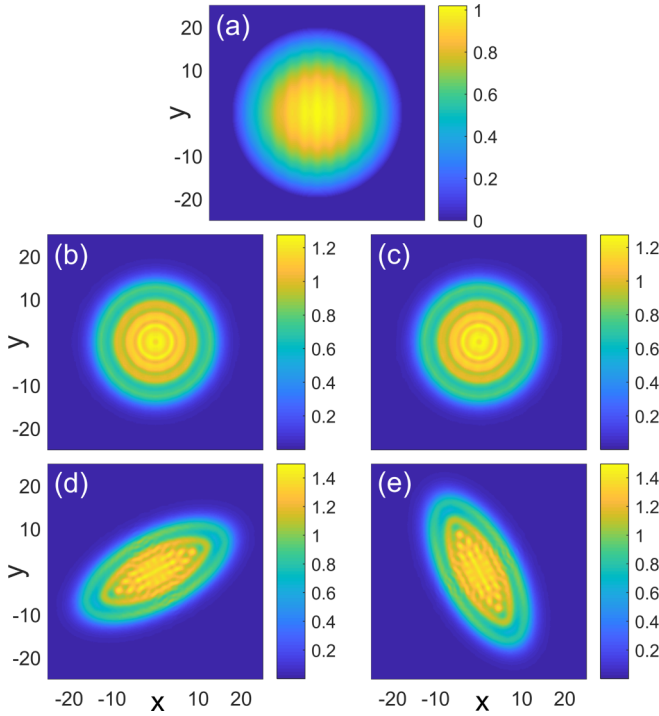


FIG. 4. (a) Density $|\psi_{20}(x, y, 0)|^2$ of initial state (10) with perturbation momentum $(k_x = 2, k_y = 0)$. (b)–(e) Density $|\psi_{20}(x, y, t = 3)|^2$ evolved with the same equations as in the Figs. 2(b)–2(e).

field kicks at $t = 0$ for \mathbf{A}_{Lx} and \mathbf{A}_{Ly} , i.e., synthetic electric field \mathbf{E}_{Lx} provides initial momentum perpendicular to the stripes of perturbation in $\psi_{10}(x, y, 0)$, while synthetic electric field \mathbf{E}_{Ly} provides initial momentum parallel to the stripes of that perturbation, which results in different dynamics of the modulation pattern later on.

Second, we consider time evolution from the initial state $\psi_{20}(x, y, 0)$ with perturbation momentum $(k_x, k_y) = (2, 0)$. Results are presented in Fig. 4; the outline of the figures is again identical to those in Figs. 2 and 3. This initial perturbation does not destabilize the trajectory, i.e., we do not observe MI in any gauge.

In a more general setting, perturbation may consist of two or more components in momentum space. As an example, we investigate the evolution of the TF initial state,

$$\tilde{\psi}_{11}(x, y, 0) = \tilde{\mathcal{N}}_{11} \psi_{\text{TF}} \{1 + 0.01[\cos(x) + \cos(y)]\}, \quad (11)$$

where $\tilde{\mathcal{N}}_{11}$ is the normalization constant determined as in Eq. (10). The initial state (11) is a superposition of perturbations with momenta $(k_x, k_y) = (1, 0)$ and $(k_x, k_y) = (0, 1)$. The MI is revealed during the time evolution for this initial state [see Fig. 5], as expected from the results for a single unstable $(k_x, k_y) = (1, 0)$ perturbation. The modulation patterns which develop during dynamics have more complex shapes than the simple modulation stripes from Fig. 3. Here, density modulations form a lattice when only the harmonic term is present [Fig. 5(b)], and this lattice is rotated in the symmetric gauge [Fig. 5(c)]. In addition to this, in both Landau gauges, the atomic cloud is elongated and rotated, which leads to nontrivial MI density patterns [Figs. 5(d) and 5(e)].

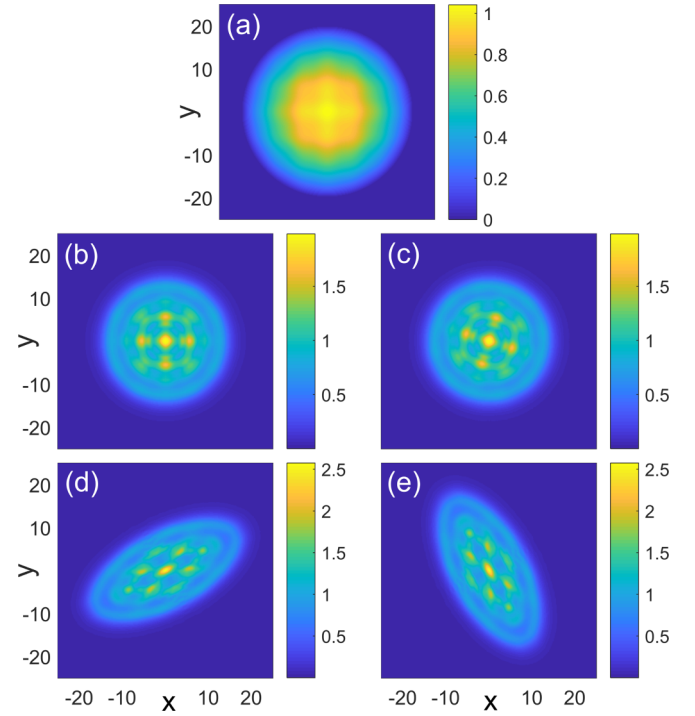


FIG. 5. (a) Density $|\tilde{\psi}_{11}(x, y, 0)|^2$ of the perturbed initial state (11). (b)–(e) Density $|\tilde{\psi}_{11}(x, y, t = 3)|^2$ evolved with the same equations as in Figs. 2(b)–2(e).

In order to have a dynamical measure of the MI phenomenon which emerges during time evolution, and numerically investigate the instability region in the momentum space of perturbations, we introduce the following quantity:

$$\Gamma_{k_x, k_y}(t) = \sqrt{\int \int [|\psi_{k_x, k_y}(x, y, t)|^2 - |\psi_{00}(x, y, t)|^2]^2 dx dy}. \quad (12)$$

In Fig. 6 we have calculated $\Gamma_{k_x, k_y}(t = 3)$ after time evolution with Eq. (9) and Eqs. (4)–(6). The (in)stability region in momentum space for evolution with the harmonic potential only [Eq. (9)] and in the symmetric gauge \mathbf{A}_S [Eq. (4)] are presented in Figs. 6(a) and 6(b), respectively. Results are indistinguishable; in both cases Γ_{k_x, k_y} has azimuthal symmetry, with the maximally unstable perturbation at radius $k = \sqrt{k_x^2 + k_y^2} \approx 0.95$. In Figs. 6(c) and 6(d), we show the (in)stability region for time evolution with the Landau gauges \mathbf{A}_{Lx} [Eq. (5)] and \mathbf{A}_{Ly} [Eq. (6)], respectively. These instability regions are of elliptical shape and perpendicular to each other. The maximally unstable perturbations in Fig. 6(c) are at $\mathbf{k} \approx (-0.55, 0.55)$ and $(0.55, -0.55)$; we can also see a drop of instability in the vicinity of $\mathbf{k} \approx (0.75, 0.75)$ and $(-0.75, -0.75)$.

More complex, direction dependent behavior of the instability region for the Landau gauges is attributed to the difference in the symmetries between the two Landau gauges and the initial TF state. The switching of the synthetic magnetic field in the Landau gauge introduces an electric field with translational symmetry; thus, it provides the momentum kick which breaks the cylindrical symmetry of the initial TF

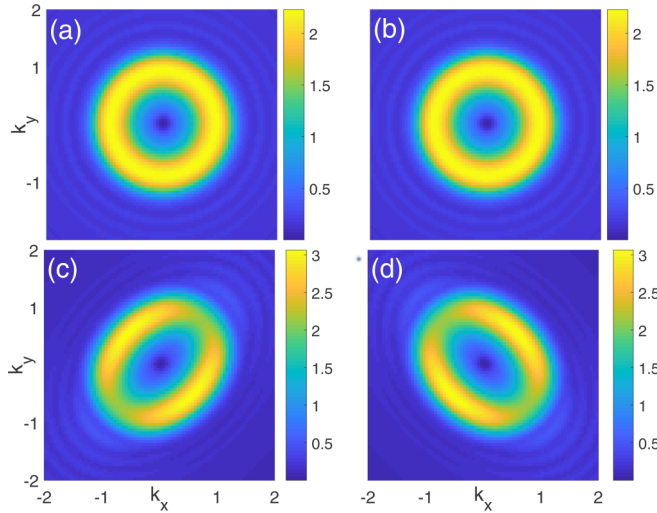


FIG. 6. Instability region in the momentum space for the time evolution with (a) the harmonic potential only [Eq. (9)], (b) the symmetric gauge \mathbf{A}_S [Eq. (4)], (c) the Landau gauge \mathbf{A}_{Lx} [Eq. (5)], and (d) the Landau gauge \mathbf{A}_{Ly} [Eq. (6)]. See text for details.

state. This further leads to the distortion of the density cloud in time, which is reflected in the momentum instability region as well. When the synthetic magnetic field is turned on in the symmetric gauge, it generates an electric field with the cylindrical symmetry; thus, the symmetry of the initial TF state is preserved during the time evolution, both in the real and the momentum space.

Up to this point, we have focused on a specific quench protocol in our study of MI: at $t = 0$, starting from a perturbed TF initial state, we turn off the harmonic trap, turn on the magnetic field, and also switch the sign of interaction. However, the quench to the system can be applied in different ways. In what follows, we comment on other foreseeable experimental scenarios. For example, we can imagine the system to be in a harmonic trap, and at $t = 0$ turn on the magnetic field and switch the sign of interaction, without turning off the harmonic confinement. We have numerically verified that keeping the trap present during the time evolution of the initially perturbed TF state does not change the results for instability regions from previous analysis in Fig. 6. In addition, we have also calculated and verified that our results are valid also when the initial state is chosen to have a Gaussian profile (perturbations are also added) with spatial width comparable to the TF state (8). In this case, the Gaussian state can be prepared as the ground state of a noninteracting system in a shallow 2D harmonic potential which is kept during the time evolution. In the next section we study another viable quench scenario.

MI of the lowest Landau level states with quench in the nonlinearity

Another interesting scenario would be to have a system prepared in the ground state with the magnetic field already present, and study the time evolution of the ground state (with perturbations added at $t = 0$) with quench in the nonlinearity. We first discuss this idea specifically for symmetric gauge: the

degenerate eigenstates

$$\psi_m(x, y) = \left(\frac{Be}{2m}\right)^{m/2} (x - iy)^m e^{-[B(x^2+y^2)/4]}, \quad (13)$$

from the lowest Landau level (LLL) have circular density profile, such that their radius increases with the angular quantum number $m = \{0, 1, 2, 3, \dots\}$ and the normalization is chosen such that the intensity has maximum value equal to 1 for each angular quantum number m .

Landau levels are flatbands and it is worthy to study MI after switching on both positive and negative nonlinearity to verify whether instability may occur for both self-focusing and self-defocusing nonlinearity. Namely, because the band is flat, one may expect that instability will occur symmetrically for both types of the nonlinearity. There are two things to comment on before we present our calculations.

First, the uniform wave is not an eigenstate of the system (as is the usual case in MI studies), because plane waves are not eigenstates of the system. Therefore, for the initial state whose instability we study, we use LLL eigenstates.

Second, we comment on the flatband intuition. It is based on the behavior of waves (light waves or matter waves) in lattices where bands at band minima, maxima, or at special points like Dirac points in graphene, have certain dispersion, that is, dependence of energy (or frequency) vs momentum (or quasimomentum). An effective low energy theory is commonly used for excitations close to these extremal points in the spectra. For example, if the dispersion is such that the effective mass is negative, one can balance dispersion of a localized wave packet with self-defocusing nonlinearity to obtain solitons. However, for the LLL, dispersion is not energy versus 2D momentum as in optical or photonic lattices, because the gauge field was involved in creating the flatbands. Therefore, that intuition is not applicable here and we are not surprised to find that MI occurs for self-focusing but not self-defocusing nonlinearity in our calculations.

In what follows we study time dynamics and the MI for each LLL eigenstate (with perturbations) after switching on the nonlinearity. The state (13) is perturbed along the azimuthal direction, so that the initial state is

$$\psi_{mn}(x, y, t = 0) = \mathcal{N}_{m,n} \psi_m(x, y) [1 + 0.01 \cos(n\phi)], \quad (14)$$

where $\phi = \arctan(y/x)$ is the polar angle and $\mathcal{N}_{m,n}$ is the normalization constant such that perturbed LLL states (14) have the same normalization as the unperturbed LLL states (13). An example of an initial state is presented in Fig. 7(a), with $m = 10$ and perturbation $n = 14$. Following the time evolution, the MI is demonstrated to occur along the azimuthal direction and only when negative (attractive) nonlinearity is switched on at $t = 0$ (here we use $\eta = -1$ and $B = 0.1$ as in previous simulations) [see Fig. 7(b)]. In order to quantify MI in momentum space, we have calculated the quantity

$$\tilde{\Gamma}_{m,n}(t) = \sqrt{\frac{\int [|\psi_{mn}(x, y, t)|^2 - |\psi_m(x, y, t)|^2]^2 dx dy}{\int |\psi_m(x, y, t)|^4 dx dy}}, \quad (15)$$

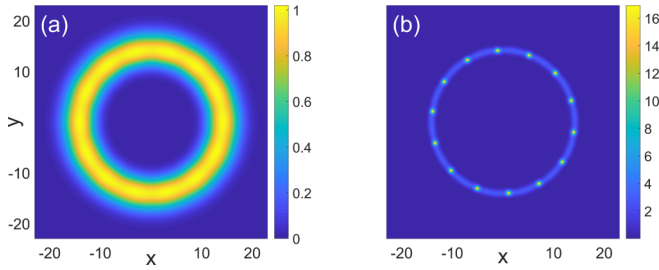


FIG. 7. (a) Density of state $\psi_{mn}(x, y, t = 0)$ in symmetric gauge with angular quantum number $m = 10$ and added perturbation $n = 14$. (b) Density profile (at $t = 3$) after time evolution from this initial state which demonstrates MI along the azimuthal direction. Here, the quench is achieved by switching on the negative nonlinearity.

which also includes the effect of different normalizations of LLL eigenstates. The results for $\tilde{\Gamma}_{m,n}(t = 3)$ (where $0 < m \leq 41$ and $0 \leq n \leq 40$) are shown in Fig. 8(a). Here, the parabolic profile of the instability region can be understood by considering the circle of maximum intensity of the eigenstate ψ_m , with radius $R_m = \sqrt{2m/B}$, as a homogeneous 1D system with periodic boundary conditions and employing textbook analysis of MI gain for 1D homogeneous systems, i.e., $g(k_{1D}) = \sqrt{2Ik_{1D}^2 - k_{1D}^4}$ [10]. In our case intensity $I = 1$ and $k_{1D} = n/R_m$ stands for the wave vector of the perturbation $\cos(n\phi)$ along the circle with radius R_m . Following this simple approach we get the relationship between quantum number m and the number n_{\max} of the perturbation with maximum gain, i.e., $m = Bn_{\max}^2/2$ which agrees excellently with results presented in Fig. 8(a). The wavelength (and wave vector) corresponding to the perturbation with maximum gain are $\lambda_{\max} = 2\pi$ (and $k_{\max} = 1$) for any $m > 0$. (A purely Gaussian symmetric gauge eigenstate with $m = 0$ does not have the ring structure as for other eigenstates and has been treated separately in a similar fashion as the TF state (10). In particular, we have not observed MI patterns for the $m = 0$ eigenstate since the spatial width of its intensity plateau is smaller than the characteristic perturbation length scale λ_{\max} , and the time dynamics leads directly to the collapse of the wave function.)

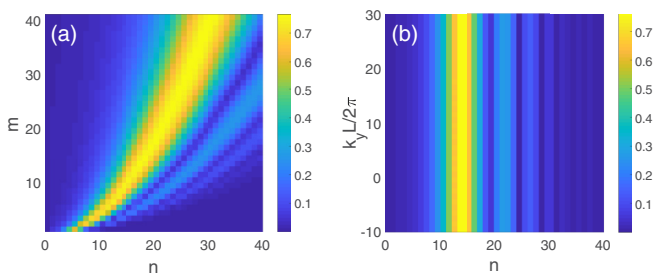


FIG. 8. Instability region in momentum space at $t = 3$ for the time evolution of LLL eigenstates following the switching on of negative nonlinearity in (a) the symmetric and (b) the Landau gauge.

A similar analysis can be made in Landau gauge. Eigenstates in the Landau gauge \mathbf{A}_{Ly} read as

$$\psi_{k_y}(x, y) = e^{ik_y y} e^{-(B/2)[x - (k_y/B)]^2}, \quad (16)$$

where k_y is the linear momentum, and we choose periodic boundary conditions, i.e., $k_y = 2\pi j/L$ with $j \in \mathbb{Z}$ and $L = 26\pi$. In this case, the density profiles of eigenstates form identical 1D stripes along the y direction which are shifted along the x direction depending on the quantum number k_y . Here, the perturbation is introduced along the y direction, and the initial state can be written as

$$\psi_{k_y n}(x, y) = \mathcal{N}_n \psi_{k_y}(x, y) \left[1 + 0.01 \cos\left(n \frac{2\pi}{L} y\right) \right]. \quad (17)$$

Once again, the MI analysis for 1D homogeneous systems can be employed, this time along the y direction, and we get $n_{\max} = L/2\pi = 13$ for the perturbation with maximum gain, in excellent agreement with numerical results for $\tilde{\Gamma}_{k_y, n}(t = 3)$ shown in Fig. 8(b).

V. CONCLUSION

In conclusion, we have explored the phenomenon of modulation instability for 2D systems which obey the NLSE in a homogeneous synthetic magnetic field. We have explored MI for the trajectory evolving from the initial state which has a Thomas-Fermi profile (8). Small perturbations upon the initial state were characterized in momentum space [Eq. (10)]. Some perturbations destabilize the trajectory, others do not, as expected. We have calculated the region of (in)stability in momentum space, as presented in Fig. 6. The stability depends on the gauge used; however, this does not mean that gauge invariance is violated. We have pointed out that when the synthetic magnetic field is turned on, there will be an instantaneous electric field kick to the system arising from Faraday's law, which depends on the gauge used; all gauges yield identical fields for $t > 0$. When an experiment is theoretically simulated, the gauge should be chosen to properly describe this initial synthetic electric field kick. We envision that our results will prove useful in studying instabilities that appear either in experiments with ultracold atomic gases, or when studying light propagation in nonlinear media, both with synthetic magnetic fields.

ACKNOWLEDGMENTS

We are grateful to Boris Malomed for useful comments. This work was supported by the Croatian Science Foundation Grant No. IP-2016-06-5885 SynthMagIA, and in part by the QuantiXLie Center of Excellence, a project cofinanced by the Croatian Government and European Union through the European Regional Development Fund—the Competitiveness and Cohesion Operational Programme (Grant No. KK.01.1.1.01.0004).

- [1] M. J. Lighthill, *J. Inst. Math. Appl.* **1**, 269 (1965).
- [2] G. B. Whitham, *J. Fluid Mech.* **22**, 273 (1965).
- [3] V. I. Bespalov and V. I. Talanov, *JETP Lett.* **3**, 307 (1966).
- [4] L. A. Ostrovskii, *Sov. Phys. JETP* **24**, 797 (1967).
- [5] T. B. Benjamin and J. E. Feir, *J. Fluid Mech.* **27**, 417 (1967).
- [6] T. B. Benjamin, *Proc. R. Soc. A* **299**, 59 (1967).
- [7] T. Taniuti and H. Washimi, *Phys. Rev. Lett.* **21**, 209 (1968).
- [8] M. Soljačić, M. Segev, T. Coskun, D. N. Christodoulides, and A. Vishwanath, *Phys. Rev. Lett.* **84**, 467 (2000).
- [9] D. Kip, M. Soljačić, M. Segev, E. E. Eugenieva, and D. N. Christodoulides, *Science* **290**, 495 (2000); J. Klinger, H. Martin, and Z. Chen, *Opt. Lett.* **26**, 271 (2000).
- [10] G. P. Agrawal, *Nonlinear Fiber Optics* (Academic, New York, 2013).
- [11] V. E. Zakharov and L. A. Ostrovsky, *Physica D* **238**, 540 (2009).
- [12] V. V. Konotop and M. Salerno, *Phys. Rev. A* **65**, 021602(R) (2002).
- [13] A. Smerzi, A. Trombettoni, P. G. Kevrekidis, and A. R. Bishop, *Phys. Rev. Lett.* **89**, 170402 (2002).
- [14] F. S. Cataliotti, L. Fallani, F. Ferlaino, C. Fort, P. Maddaloni, and M. Inguscio, *New J. Phys.* **5**, 71 (2003).
- [15] G. Theocharis, Z. Rapti, P. G. Kevrekidis, D. J. Frantzeskakis, and V. V. Konotop, *Phys. Rev. A* **67**, 063610 (2003).
- [16] J. H. Nguyen, D. Luo, and R. G. Hulet, *Science* **356**, 422 (2017).
- [17] P. J. Everitt, M. A. Sooriyabandara, M. Guasoni, P. B. Wigley, C. H. Wei, G. D. McDonald, K. S. Hardman, P. Manju, J. D. Close, C. C. N. Kuhn, S. S. Szigeti, Y. S. Kivshar, and N. P. Robins, *Phys. Rev. A* **96**, 041601(R) (2017).
- [18] Z. Chen, M. Segev, and D. N. Christodoulides, *Rep. Prog. Phys.* **75**, 086401 (2012).
- [19] J. Dalibard, F. Gerbier, G. Juzeliūnas, and P. Öhberg, *Rev. Mod. Phys.* **83**, 1523 (2011).
- [20] N. Goldman, G. Juzeliūnas, P. Öhberg, and I. B. Spielman, *Rep. Prog. Phys.* **77**, 126401 (2014).
- [21] N. R. Cooper, J. Dalibard, and I. B. Spielman, *Rev. Mod. Phys.* **91**, 015005 (2019).
- [22] L. Lu, J. D. Joannopoulos, and M. Soljačić, *Nat. Photonics* **8**, 821 (2014).
- [23] T. Ozawa, H. M. Price, A. Amo, N. Goldman, M. Hafezi, L. Lu, M. C. Rechtsman, D. Schuster, J. Simon, O. Zilberberg, and I. Carusotto, *Rev. Mod. Phys.* **91**, 015006 (2019).
- [24] R. Dum and M. Olshanii, *Phys. Rev. Lett.* **76**, 1788 (1996).
- [25] K. W. Madison, F. Chevy, W. Wohlleben, and J. Dalibard, *Phys. Rev. Lett.* **84**, 806 (2000).
- [26] J. R. Abo-Shaeer, C. Raman, J. M. Vogels, and W. Ketterle, *Science* **292**, 476 (2001).
- [27] Y.-J. Lin, R. L. Compton, K. Jiménez-García, J. V. Porto, and I. B. Spielman, *Nature (London)* **462**, 628 (2009).
- [28] M. Aidelsburger, M. Atala, S. Nascimbene, S. Trotzky, Y.-A. Chen, and I. Bloch, *Phys. Rev. Lett.* **107**, 255301 (2011).
- [29] J. Struck, C. Ölschläger, M. Weinberg, P. Hauke, J. Simonet, A. Eckardt, M. Lewenstein, K. Sengstock, and P. Windpassinger, *Phys. Rev. Lett.* **108**, 225304 (2012).
- [30] H. Miyake, G. A. Siviloglou, C. J. Kennedy, W. C. Burton, and W. Ketterle, *Phys. Rev. Lett.* **111**, 185302 (2013).
- [31] M. Aidelsburger, M. Atala, M. Lohse, J. T. Barreiro, B. Paredes, and I. Bloch, *Phys. Rev. Lett.* **111**, 185301 (2013).
- [32] G. Jotzu, M. Messer, R. Desbuquois, M. Lebrat, and T. Uehlinger, D. Greif, and T. Esslinger, *Nature (London)* **515**, 237 (2014).
- [33] M. C. Rechtsman, J. M. Zeuner, A. Tünnermann, S. Nolte, M. Segev, and A. Szameit, *Nat. Photonics* **7**, 153 (2013).
- [34] M. C. Rechtsman, J. M. Zeuner, Y. Plotnik, Y. Lumer, D. Podolsky, F. Dreisow, S. Nolte, M. Segev, and A. Szameit, *Nature (London)* **496**, 196 (2013).
- [35] M. Hafezi, S. Mittal, J. Fan, A. Migdall, and J. M. Taylor, *Nat. Photonics* **7**, 1001 (2013).
- [36] Y. Yang, C. Peng, D. Zhu, H. Buljan, J. D. Joannopoulos, B. Zhen, and M. Soljačić, *Science* **365**, 1021 (2019).
- [37] R. O. Umucalılar and I. Carusotto, *Phys. Rev. A* **84**, 043804 (2011).
- [38] M. Hafezi, E. A. Demler, M. D. Lukin, and J. M. Taylor, *Nat. Phys.* **7**, 907 (2011).
- [39] K. Fang, Z. Yu, and S. Fan, *Nat. Photonics* **6**, 782 (2012).
- [40] S. Longhi, *Opt. Lett.* **38**, 3570 (2013).
- [41] T. Dubček, K. Lelas, D. Jukić, R. Pezer, M. Soljačić, and H. Buljan, *New J. Phys.* **17**, 125002 (2015).
- [42] D. C. Tsui, H. L. Stormer, and A. C. Gossard, *Phys. Rev. Lett.* **48**, 1559 (1982).
- [43] R. B. Laughlin, *Phys. Rev. Lett.* **50**, 1395 (1983).
- [44] O. Manela, M. Segev, D. N. Christodoulides, and D. Kip, *New J. Phys.* **12**, 053017 (2010).
- [45] Y. Lumer, Y. Plotnik, M. C. Rechtsman, and M. Segev, *Phys. Rev. Lett.* **111**, 243905 (2013).
- [46] D. Leykam and Y. D. Chong, *Phys. Rev. Lett.* **117**, 143901 (2016).
- [47] D. D. Solnyshkov, O. Bleu, B. Teklu, and G. Malpuech, *Phys. Rev. Lett.* **118**, 023901 (2017).
- [48] J. L. Marzuola, M. C. Rechtsman, B. Osting, and M. A. Bandres, *arXiv:1904.10312*.
- [49] D. A. Smirnova, L. A. Smirnov, D. Leykam, and Y. S. Kivshar, *Laser Photonics Rev.* **13**, 1900223 (2009).
- [50] S. Kruk, A. Poddubny, D. Smirnova, L. Wang, A. Slobozhanyuk, A. Shorokhov, I. Kravchenko, B. Luther-Davies, and Y. Kivshar, *Nat. Nanotechnol.* **14**, 126 (2019).
- [51] Y. Wang, L. Lang, C. H. Lee, B. Zhang, and Y. D. Chong, *Nat. Commun.* **10**, 1102 (2019).
- [52] P. St-Jean, V. Goblot, E. Galopin, A. Lemaitre, T. Ozawa, L. Le Gratiet, I. Sagnes, J. Bloch, and A. Amo, *Nat. Photonics* **11**, 651 (2017).
- [53] B. Bahari, A. Ndao, F. Vallini, A. El Amili, Y. Fainman, and B. Kanté, *Science* **358**, 636 (2017).
- [54] M. A. Bandres, S. Wittek, G. Harari, M. Parto, J. Ren, M. Segev, D. N. Christodoulides, and M. Khajavikhan, *Science* **359**, eaar4005 (2018).
- [55] Y. Hadad, A. B. Khanikaev, and A. Alù, *Phys. Rev. B* **93**, 155112 (2016).
- [56] O. Bleu, D. D. Solnyshkov, and G. Malpuech, *Phys. Rev. B* **93**, 085438 (2016).

- [57] D. A. Dobrykh, A. V. Yulin, A. P. Slobozhanyuk, A. N. Poddubny, and Yu. S. Kivshar, *Phys. Rev. Lett.* **121**, 163901 (2018).
- [58] A. Bisianov, M. Wimmer, U. Peschel, and O. A. Egorov, *Phys. Rev. A* **100**, 063830 (2019).
- [59] L. Pitaevskii and S. Stringari, *Bose-Einstein Condensation* (Clarendon, Oxford, 2013).
- [60] L. J. LeBlanc, K. Jiménez-García, R. A. Williams, M. C. Beeler, W. D. Phillips, and I. B. Spielman, *New J. Phys.* **17**, 065016 (2015).
- [61] C. Chin, R. Grimm, P. Julienne, and E. Tiesinga, *Rev. Mod. Phys.* **82**, 1225 (2010).
- [62] E. Ott, *Chaos in Dynamical Systems* (Cambridge University Press, Cambridge, 1993).